Interface Dipole and Growth Mode of Partially and Fully Fluorinated Rubrene on Au(111) and Ag(111)

ARTICLE *in* THE JOURNAL OF PHYSICAL CHEMISTRY C · FEBRUARY 2015

Impact Factor: 4.77 · DOI: 10.1021/jp511822g

THE JOURNAL OF PHYSICAL CHEMISTRY C

Article

pubs.acs.org/JPCC

Interface Dipole and Growth Mode of Partially and Fully Fluorinated Rubrene on Au(111) and Ag(111)

F. Anger,[†] H. Glowatzki,[‡] A. Franco-Cañellas,[†] C. Bürker,[†] A. Gerlach,[†] R. Scholz,[¶] Y. Sakamoto,[§] T. Suzuki,[§] N. Koch,[‡,#] and F. Schreiber*[,†]

[†]Institut für Angewandte Physik, Universität Tübingen, 72076 Tübingen, Germany

[‡]Helmholtz-Zentrum für Materialien und Energie GmbH, Hahn-Meitner-Platz 1, 14109 Berlin, Germany

[¶]Institut für Angewandte Photophysik, TU Dresden, 01069 Dresden, Germany

[§]Institute for Molecular Science, 5-1 Higashiyama, Myodaiji, Okazaki 444-8787, Japan

[#]Humboldt-Universität zu Berlin, Institut für Physik, 12489 Berlin, Germany

ABSTRACT: Thin films of fully and partially fluorinated rubrene deposited on Au(111) and Ag(111) were investigated using ultraviolet and X-ray photoelectron spectroscopy. We demonstrate that fluorination of the molecules is an efficient way for tuning the metal−organic interface dipole and the hole injection barrier. Moreover, the results indicate that the pronounced electrostatic dipole moment of partially fluorinated rubrene (F_{14}-RUB) has a strong impact on the growth mode of these molecules. Most notably, we infer that the first layer of F_{14}-RUB on Au(111) and Ag(111) is formed by molecules with alternating orientation of their dipole moments whereas the second layer shows a nearly uniform orientation.

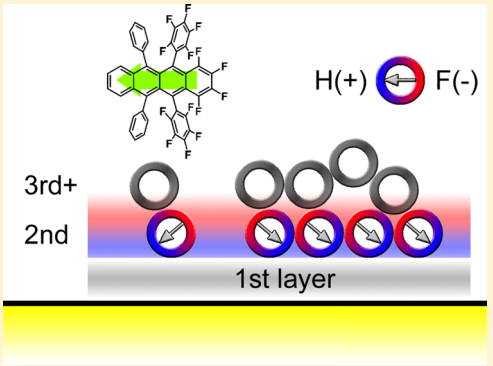

INTRODUCTION

One of the most promising materials for organic electronics among small molecule organic semiconductors is rubrene ($C_{42}H_{28}$, RUB), which is known for its high charge carrier mobility.[1−5] For the application in organic devices, it is a key point to combine good charge carrier properties of a material with a suitable energy level alignment at its interface.[6,7] To this end, the controlled manipulation of the semiconductor interface by orienting the molecular dipoles is of high interest.[8−11] One of the most efficient ways to tune the electronic energy level alignment of organic semiconductors is partial or complete fluorination.[12−15] With the same molecular geometry as RUB, the newly synthesized perfluoro-5,6,11,12-tetraphenyltetracene ($C_{42}F_{28}$, PF-RUB) and 1,2,3,4-tetrafluoro-5,12-bis(2,3,4,5,6-pentafluorophenyl)-6,11-diphenyltetracene ($C_{42}F_{14}H_{14}$, F_{14}-RUB) molecules provide an electronic structure that is very different (Figure 1). Moreover, F_{14}-RUB is of particular interest for the manipulation of organic interfaces, since it provides a large intrinsic dipole moment.[16] Measurements of the optical band gap as well as density functional theory (DFT) calculations of the electronic energy levels of these molecules have already been performed,[16] but an experimental determination of the position of the absolute energy levels of the materials is still missing. For the three different molecules we find a gradual increase of the ionization potential with the degree of fluorination. Interestingly, for F_{14}-RUB we observe a nonmonotonic shift of the work function and the hole injection barrier (HIB) with increasing film thickness, which is accompanied by a nonmonotonic shift of all energy levels.

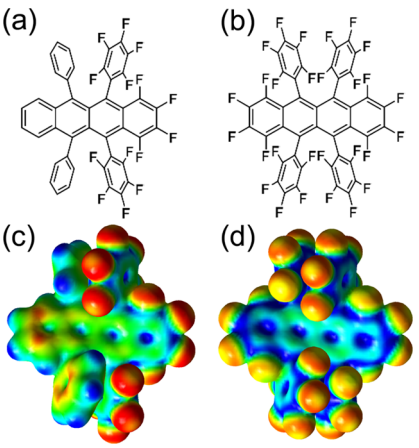

Figure 1. Panel (a) and (b) show the chemical structure, (c) and (d) the molecular electrostatic potential of F_{14}-RUB ($C_{42}F_{14}H_{14}$) and PF-RUB ($C_{42}F_{28}$), respectively. In contrast to RUB and PF-RUB, F_{14}-RUB exhibits a large static dipole moment along its backbone.

Received: November 26, 2014
Revised: February 20, 2015

DOI: 10.1021/jp511822g
J. Phys. Chem. C XXXX, XXX, XXX−XXX

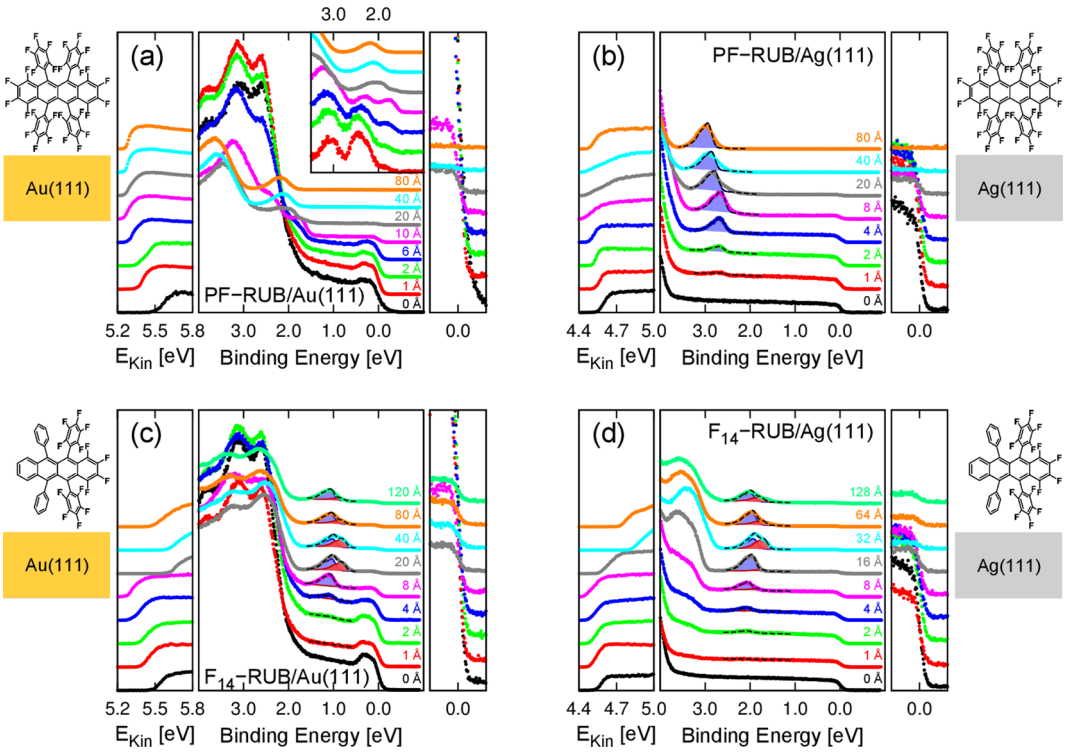

Figure 2. Valence spectra of PF-RUB on (a) Au(111) and (b) Ag(111) and of F_{14}-RUB on (c) Au(111) and (d) Ag(111). The HOMO peak of PF-RUB on Ag(111) is fitted with one (blue), the HOMO peak of F_{14}-RUB with two (blue and red) vibronic progressions, according to eq 1. The subfigures on the left of each spectrum show the secondary electron cutoff. On the right of the spectra a zoom into the region of the Fermi-edge is provided. In order to detect the HOMO peak of PF-RUB on Au(111), the spectrum of the pristine substrate was subtracted (inset of a).

EXPERIMENTAL SECTION

Ultraviolet photoelectron spectroscopy (UPS) and X-ray photoelectron spectroscopy (XPS) measurements were performed at the SurIcat beamline of BESSY II in Berlin using a Scienta SES 100 electron analyzer. Sample preparation proceeded in a preparation chamber (base pressure < 2×10^{-9} mbar), which was connected to an analysis chamber (base pressure <5×10^{-10} mbar) allowing sample transfer without breaking UHV conditions. Clean Au(111) and Ag(111) crystals were prepared by repeated cycles of Ar^+ sputtering and annealing to 450 °C before thin film deposition. The surface cleanliness was confirmed by XPS. The materials were synthesized and purified by temperature gradient sublimation. Thin film growth was performed at a base pressure of 2×10^{-9} mbar at room temperature and controlled by a quartz crystal microbalance. UPS (XPS) measurements were performed with $h\nu$ = 35 eV (1200 eV) photon energy at normal incidence. The secondary electron cutoff (SECO) was measured at −10 V sample bias. The measured work functions for the clean substrates are 5.48 eV for Au(111) and 4.55 eV for Ag(111), which is in good agreement with previously reported values.[17,18]

RESULTS

Valence Spectra. Figure 2 shows the valence spectra of PF-RUB and F_{14}-RUB on Au(111) and Ag(111). Generally, upon deposition of PF-RUB and F_{14}-RUB, we observe a decrease of the prominent metal valence band states at binding energies E_B > 2 eV for Au(111) and E_B > 4 eV for Ag(111), respectively, while at the same time new peaks related to the molecular electronic states appear.

Photoemission peaks were fitted with a vibronic progression with its center of mass at E_0

$$I(E) = A \sum_n \frac{S^n}{n!} \frac{1}{\sigma_n \sqrt{2\pi}} \exp\left[- \frac{(E_0 + \Delta E - E)^2}{2\sigma_n^2} \right] \quad (1)$$

as it has been suggested for HOMO−LUMO transitions of the same materials,[16] using the Gaussian width σ_i and spacing of the vibronic progression ΔE as fit parameters. Particularly for the Huang−Rhys parameter S = 0.6 we used the value obtained from angle-resolved UPS measurements on RUB.[19]

For the spectra of PF-RUB on Au(111), we carefully subtract the clean metal spectrum from each recorded spectrum, since many of the interesting features are superimposed by peaks of the underlying metal. The background-subtracted spectra of PF-RUB on Au(111) are depicted in the inset of Figure 2a. Despite the remaining substrate-derived artifact at $E_B \sim 2.40$ eV, this enables us to determine the HOMO onset at approximately 1.60 eV for lower film thicknesses. The onset moves with increasing film thickness to $E_B \sim 1.80$ eV binding energy up to the maximum film thickness of 80 Å (Figure 6).

For PF-RUB on Ag(111) (Figure 2b), the HOMO onset is found at $E_B \sim 2.40$ eV for nominal coverages below 5 Å and shifts to 2.60 eV for a thickness of 80 Å. The position of the HOMO onset of PF-RUB on both metals is found to be at a substantially lower binding energy than has been observed for the hydrogenated RUB.[20−22]

In the case of F_{14}-RUB, we find the HOMO onset at E_B = 0.85 eV on Au(111) and 1.75 eV on Ag(111) at a nominal thickness of 4 Å, as can be seen in Figure 2c and d. Thus, the HOMO of F_{14}-RUB on Au(111) and Ag(111) lies between the corresponding values for PF-RUB and RUB.[20,21] This is

DOI: 10.1021/jp511822g
J. Phys. Chem. C XXXX, XXX, XXX−XXX

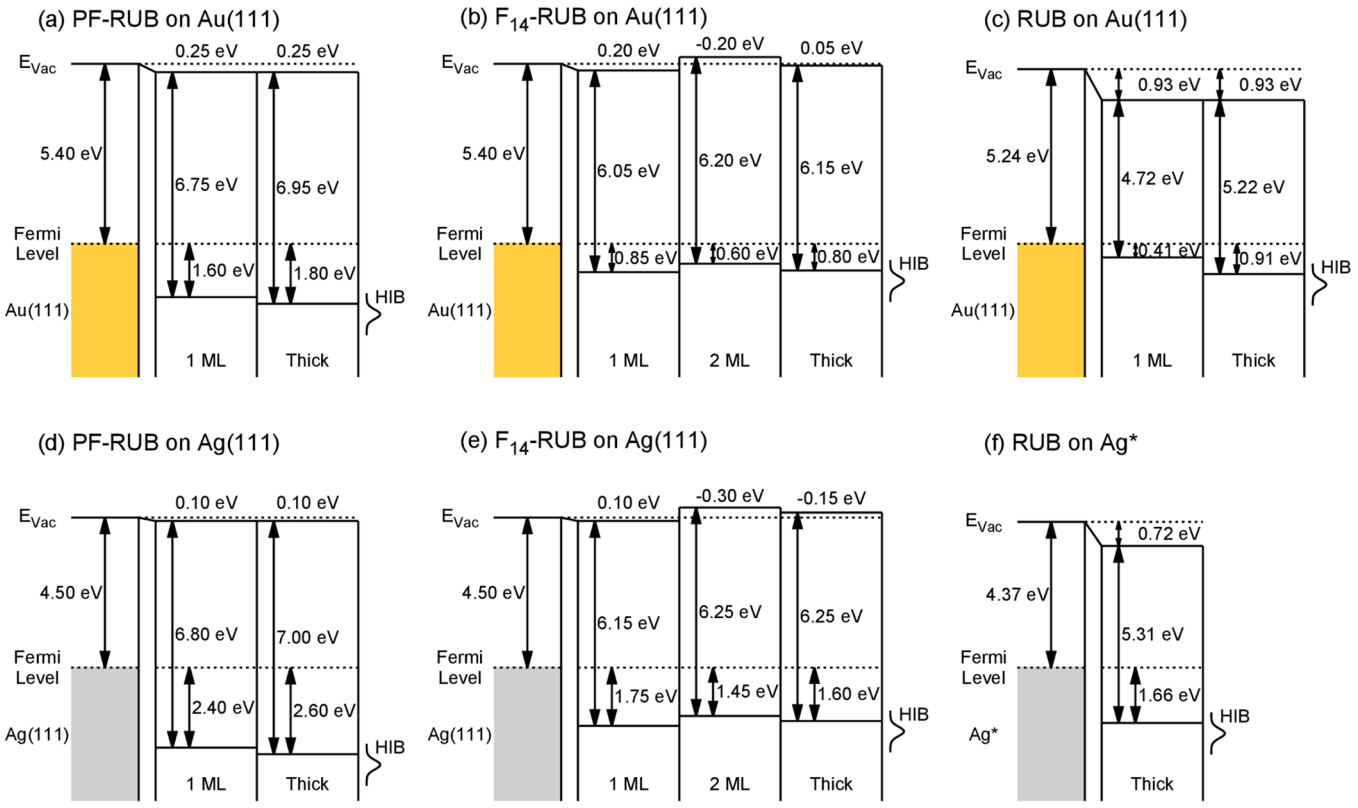

Figure 3. Energy level alignment of PF-RUB, F_{14}-RUB, and RUB on Au(111), (a), (b), and (c), respectively, and on Ag(111), (d), (e), and (f), respectively. The hole injection barriers (HIBs) of the thin films are shown in relation to the vacuum (E_{Vac}) and Fermi level. The energy difference between the HOMO onset and the Fermi level thereby defines the HIB. Values for schematics (c) and (f) are taken from refs 20 and 21 (*no UPS data is available for RUB on Ag(111)), respectively. Note that F_{14}-RUB does not show a monotonic shift in the alignment with increasing layers.

qualitatively in good agreement with the behavior predicted by DFT calculations[16] and shows the tunability of the absolute energy levels of the RUB molecule by partial and complete substitution with fluorine. Note, however, that F_{14}-RUB essentially differs from RUB and PF-RUB due to a strong dipole moment along its backbone, generated by its geometry.

On both substrates at a thickness of approximately 20 Å, a new HOMO peak appears as a shoulder of the previously observed HOMO.[11,23] The new HOMO becomes dominant over the former HOMO at roughly 24 Å and vanishes again for thicker films. In order to quantify this observation, we fitted the resulting broad HOMO with two peaks according to eq 1 with an offset of 0.2 eV from each other. The resulting position of the HOMO onset shifts toward the Fermi-edge with increasing molecular thickness, reaching E_B = 0.60 eV on Au(111) and 1.45 eV on Ag(111) at about 20 Å and moves slightly toward again higher binding energy for thicker films. At 120 Å we determine the HOMO onset at 0.80 eV (1.60 eV) for F_{14}-RUB on Au(111) (Ag(111)).

In order to study the coverage behavior of the molecules on the substrate, we also take a closer look at the Fermi-edge. At the right-hand side of Figure 2a–d, the intensity at the Fermi-edge of the respective measurements is shown in more detail. While the Fermi-edge vanishes for PF-RUB deposited on Au(111) and Ag(111) at higher nominal coverages, we still observe a pronounced Fermi-edge for F_{14}-RUB even at the highest investigated film thicknesses.

Figures 2a–d show the secondary electron cutoff of the respective samples, which reflects the change in the work function. Upon completion of the first nominal monolayer (~8 Å) of PF-RUB, the work function decreases by about 0.25 eV on Au(111) and 0.10 eV on Ag(111). It remains constant for all thicknesses above the first monolayer.

During the formation of the first nominal layer of F_{14}-RUB, we observe a similar decrease of the work function, with about 0.20 eV on Au(111) and 0.10 eV on Ag(111). Upon the formation of the nominal second layer of F_{14}-RUB we observe—in strong contrast to PF-RUB—a linear increase of the work function on both metals. At about 24 Å a maximum work function increase of roughly 0.40 eV compared to the first nominal layer is reached for Au(111) and Ag(111). With further deposition the work function slightly decreases again and is found at 0.05 eV (−0.15 eV) for F_{14}-RUB on Au(111) (Ag(111)) for 120 Å. A schematic of the energy level alignment of PF-RUB and F_{14}-RUB on both Au(111) and Ag(111) relative to the vacuum energy E_{Vac} is given in Figure 3.

Core-Level Spectra. In order to investigate the chemical composition and electronic states of the molecules, XPS measurements were performed. Spectra were recorded at the energies of the C 1s, F 1s, and respective dominant metal core-levels (Au 4f and Ag 3d). Figure 4 shows the XPS results of PF-RUB and F_{14}-RUB on Au(111) and Ag(111).

For all samples we observe one peak in the F 1s region. In the C 1s region two peaks appear for PF-RUB and three peaks for F_{14}-RUB on both metals. These chemically shifted peaks are designated as C 1s (i), (ii), and (iii) where the C 1s (ii) peak of F_{14}-RUB occurs only as a shoulder of the C 1s (iii) peak. The different peaks originate from the nonequivalent binding sites within the molecules. For both molecules every carbon atom is bound to three further atoms, of which at least two are carbon

DOI: 10.1021/jp511822g
J. Phys. Chem. C XXXX, XXX, XXX−XXX

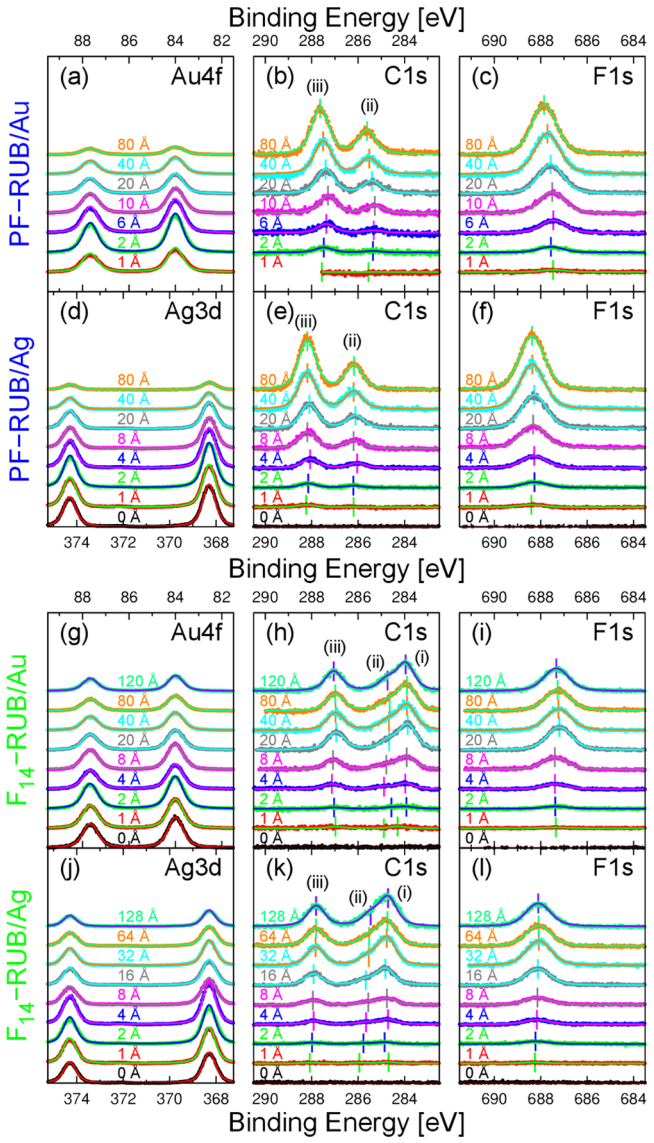

Figure 4. Core-level spectra of PF-RUB on Au(111) (a–c) and Ag(111) (d–f) and F_{14}-RUB on Au(111) (g–i) and Ag(111) (j–l). The Shirley background of the peaks is removed. The spectra are fitted using Voigt profile, with constant width and Gaussian/Lorentzian ratio for each species of peak, i.e., metal, C 1s, and F 1s. Peak positions of the C 1s and F 1s peaks are marked with a short vertical line. Whereas PF-RUB shows two C 1s peaks, (i) and (ii), we observe a third peak (iii) for F_{14}-RUB. For further explanation, see text. Note that the metal peaks decrease less in intensity with increasing film thickness for F_{14}-RUB than for PF-RUB.

atoms. The C 1s (i), (ii), and (iii) peaks are assigned to carbon atoms bound to a fluorine, carbon, and hydrogen, respectively, as their third binding partner.

This assignment is corroborated by density functional calculations with the B3LYP hybrid functional performed with Turbomole 6.4:[24] The sequence of C 1s core-levels in PF-RUB and F_{14}-RUB is reproduced, giving a splitting of 1.6 eV in PF-RUB (corresponding to (i)–(ii), observed 2.0 eV). For F_{14}-RUB the splitting between the C atoms bound to either H or F is calculated to 2.8 eV (corresponding to (i)–(iii), observed 3.1 eV), the C atoms surrounded by three carbons occurring in between, as observed (ii). Due to the B3LYP functional and the TZVP basis set used, the binding energies of all core-levels are underestimated by about 7 eV with respect to the experimental findings, in the same range as in previous B3LYP/SV(P) calculations for PTCDA.[25] Despite this systematic offset of the DFT calculations, the relative shifts between C atoms with different bond configurations in PF-RUB and F_{14}-RUB remain quite reliable. Note that the calculated core-levels of the two possible isomers[16] of either F_{14}-RUB (C_2, C_s) or PF-RUB (D_2, C_{2h}) are so similar that these isomers cannot be distinguished by analyzing the measured XPS spectra with a fwhm of about 0.7 eV.

For a quantitative analysis all amplitudes and binding energies were fitted using a Voigt profile. The widths were fixed for each specific peak (i.e., Au 4f, Ag 3d, C 1s, F 1s). Weighting the ratio of the integrated C 1s and F 1s peak intensities with the sensitivity factors and the transmission of the electron analyzer, the ratio of carbon to fluorine atoms can be determined experimentally.[26] We find a ratio of ~3 for F_{14}-RUB and ~1.5 for PF-RUB, which is in good agreement with the ratio of carbon and fluorine atoms in the respective molecules (Figure 5).

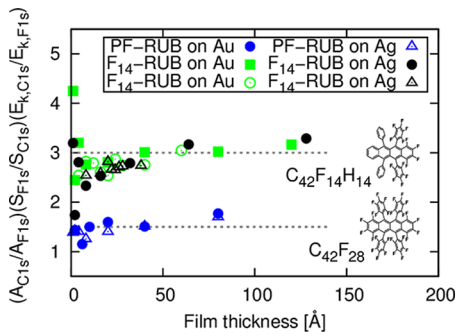

Figure 5. Comparing the areas A_C and A_F of the C 1s and F 1s peaks, we can confirm the ratio of the number of C and F atoms in the molecules from the XPS measurements. Using $(A_{C1s}/A_{F1s})(S_{F1s}/S_{C1s})(E_{k,C1s}/E_{k,F1s})$ we insert (S_{F1s}/S_{C1s}) = 2.87 for the ratio of the sensitivity factors and the ratio of the kinetic energies $(E_{k,C1s}/E_{k,F1s})$ = 1.78 in order to account for the transmission function of the electron analyzer. We obtain a ratio of ~3 for F_{14}-RUB and ~1.5 for PF-RUB, which corresponds nicely to the ratio of C to F atoms in the respective molecules. The gray dotted lines are a guide for the eye.

For both materials we observe a rigid shift of all energy levels with increasing film thickness. This indicates that the molecules do not interact strongly with the substrate and are only weakly bound.[27,28] The resulting curves for PF-RUB are found in Figure 6 and for F_{14}-RUB in Figure 7. The plot for F_{14}-RUB comprises green open and black closed circles denoting two sets of data of two respective samples. The second (black) curve was taken to measure the interesting region of 20–40 Å in more detail (corresponding raw spectra are not shown here).

DISCUSSION

In the case of PF-RUB on both metals, we observe a complete disappearance of the Fermi-edge (cf. Figure 2a and b) as well as rapidly decreasing intensities of the metal core-levels (Figure 4a and d) with increasing film thickness. This indicates that the metal surface is completely covered by a closed layer of molecules, analogously to RUB grown on the same substrates.[20,21] Thus, the molecules grow either layer-by-layer (Frank–van der Merve) or, as observed for RUB, layer-plus-island (Stranski–Krastanov).[22,29] In contrast, for F_{14}-RUB the

DOI: 10.1021/jp511822g
J. Phys. Chem. C XXXX, XXX, XXX–XXX

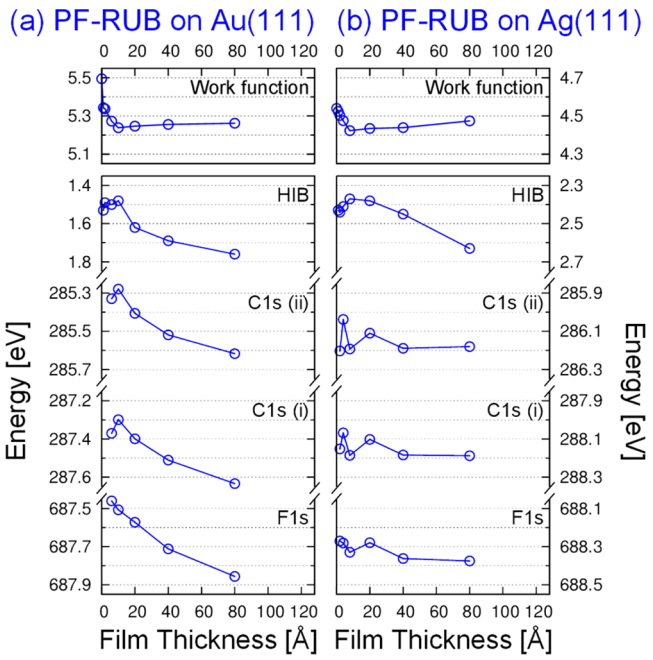

Figure 6. Energy level alignment of work function, HIB, and core-levels (C 1s and F 1s) depending on the film thickness for PF-RUB. Panel (a) shows the results on Au(111) and (b) on Ag(111). For both metal substrates, the respective energy levels show the same trends with thickness. The values are obtained from the fit results of Figures 2 and 4.

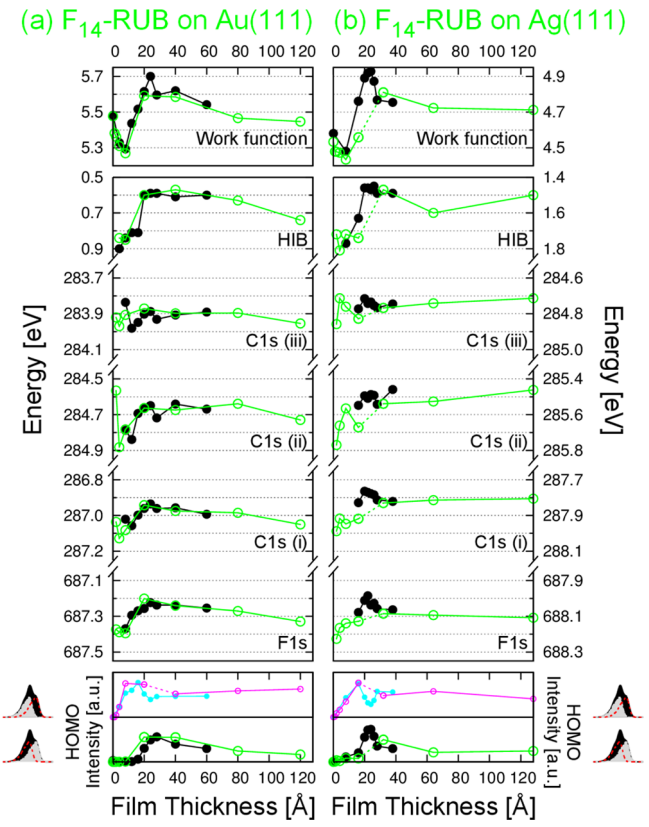

Figure 7. Energy level alignment of work function, HIB, and core-levels (C 1s and F 1s) depending on the film thickness, for F_{14}-RUB. Panel (a) shows the results on Au(111) and (b) on Ag(111). Green and black (together with pink and cyan) stand for two different samples. Whereas the values for the green (and pink) sample give an overview over general trends, black (and cyan) data points focus particularly on the nominal thickness below 40 Å. For both metal substrates, the respective energy levels show the same trends with thickness. The values are obtained from the fit results of Figures 2 and 4. The graphs at the very bottom show the intensity of the two vibronic progressions used for fitting the HOMO peak in the UPS. The new HOMO (green/black curves in lowest graph) rises particularly above ~20 Å, and the former HOMO (pink/cyan curves) loses intensity. At roughly 40 Å the new HOMO vanishes. The new HOMO is shifted by 0.2 eV toward the Fermi-edge, the green curve corresponds to the pink curve, and black corresponds to cyan.

Fermi-edge remains clearly visible even at the highest coverage (cf. Figure 2c and d), and also the intensities of the metal core-levels show a less distinct dependence on the film thickness (Figure 4g and j) compared to PF-RUB. This indicates strong island growth (Vollmer–Weber) which is often found for organic molecules on metals.[30−32] It plays a crucial role for the evaluation of the data of F_{14}-RUB, since the spectral features of possibly lower lying layers have to be considered for each measurement.

PF-RUB on Au(111) and Ag(111). For PF-RUB on Au(111) (Figure 6a) we observe an almost linear decrease $\Delta\phi$ in the work function up to a nominal thickness of 8 Å, which we assign to the formation of the first monolayer. This decrease can be explained by the so-called push-back effect.[33−35] For RUB on Au(111) $\Delta\phi$ =−0.93 eV[20] and for pentacene on Au(111) $\Delta\phi$ =−0.95 eV[36] have been reported. For PF-RUB we measure a decrease of only $\Delta\phi$ =−0.25 eV which is significantly smaller. This difference could be explained by a larger bonding distance caused by the perfluorination of the molecule as it has been explained for perfluoropentacene on Au(111)[36] and on Cu(111).[37] With further increase of the film thickness the work function remains constant. This means that after completion of the first layer the surface dipole is not modified by additional molecules and hence no change in the work function occurs. For the hole injection barrier (HIB), a linear trend up to 8 Å can be observed. Upon completion of the first layer the HIB decreases by roughly 0.20 eV. This shift can be fully explained by the screening of the photohole.[38] Further increase of the film thickness leads to an apparent increase of the HIB by up to 0.35 eV at 80 Å which seemingly saturates for higher molecular depositions. This can again be explained by photohole screening. In this case, the vanishing contribution of the metal to the screening is the driving factor. With increasing film thickness the photohole is less screened, and in turn the HIB seemingly increases.

For PF-RUB on Ag(111) (Figure 6b), we find qualitatively the same behavior and the same arguments hold. Up to nominal 8 Å film thickness the work function decreases by $\Delta\phi$ =−0.10 eV, which again is much lower than $\Delta\phi$ =−0.72 eV reported for RUB on Ag(111).[21] In contrast to Au(111), the core-levels do not follow exactly the same trends of the HIB for the film on Ag(111). A possible explanation could be a slightly rougher growth mode on Ag(111), thus allowing to observe more contribution of lower layers to the XPS core-levels even at higher nominal film thickness.

F_{14}-RUB on Au(111) and Ag(111). For F_{14}-RUB the interpretation of its growth is more complex than for PF-RUB or RUB due to its strong intrinsic dipole moment along the long molecular axis.[16] In Figure 7a and b the results for F_{14}-RUB on Au(111) and Ag(111) are shown, respectively. Since the phenomena observed for both metals are qualitatively identical, the following discussion exemplarily refers to only

DOI: 10.1021/jp511822g
J. Phys. Chem. C XXXX, XXX, XXX−XXX

F_{14}-RUB on Au(111). Similarly to PF-RUB, we observe a linear decrease of the work function up to a nominal thickness of 8 Å which refers to the formation of the first layer. The absolute value of $\Delta\phi$ =−0.20 eV is virtually identical to that of PF-RUB on the same substrate. Obviously, very similar to PF-RUB, a push-back effect occurs that can be explained by a larger distance of F_{14}-RUB to the substrate compared to RUB. Surprisingly, in the first layer the large static dipole moment of the molecule, which we expect to result in a drastically changed work function compared to PF-RUB, does not come into effect.

For RUB, the complex three-dimensional structure of the molecule leads to intricate structures and superstructures as reported for RUB on Au(111) and Ag(111).[28,39−42] Deposited on Au(111), it was found that the molecules orient themselves with a tilt angle of their twisted backbone of roughly 40° relative to the surface.[43,44] Due to the similar geometry of the molecules, it appears reasonable that also PF-RUB and F_{14}-RUB molecules align themselves in a similar twisted and inclined conformation for their first layers on the metal. If the F_{14}-RUB molecules, however, do not lie flatly on the surface, there is a component of their static dipole moment perpendicular to the substrate surface. Showing a very similar behavior as PF-RUB monolayers (without static dipole moment), F_{14}-RUB molecules seem to adsorb in an arrangement which neutralizes the overall dipole within the first layer. This suggests an alternating arrangement[10,11] as shown in Figure 8, where the molecules are inclined with respect to the surface. Adjacent molecules have inverted orientation in this configuration that results in an overall zero dipole moment perpendicular to the substrate surface.

Between 8 and 24 Å nominal thickness we observe a distinct increase of the work function. This can be related to the growth beyond the first monolayer. The work function change compared to the first layer reaches a maximum of $\Delta\phi$ = +0.40 eV. This points to the formation of a dipole moment within the second molecular layer. Hence, we propose that the molecules within the second layer are inclined with their fluorinated end (− partial charges) pointing away from the surface. This leads to a dipole moment perpendicular to the surface plane which becomes gradually stronger with the increasing number of molecules within the second layer.

In order to estimate this increase of the work function, we consider a simple model using the intrinsic dipole moment d = 4.2 D along the backbone of the molecule, as obtained from DFT calculations for the twisted conformation of F_{14}-RUB.[16] If we furthermore describe the molecule with a sphere of 10 Å diameter being densely packed (surface density N_{dip} = 1.155 × 10^{18} m^{-2}) and tilted with its backbone by 40°, we can find an upper limit for the effective intrinsic dipole moment of the molecules in the second layer using the Helmholtz equation[37]

$$\Delta\phi = \frac{ed\cdot \sin(40\ ^\circ)N_{dip}}{\varepsilon_r\varepsilon_0} = 1.17/\varepsilon_r \text{ eV} \quad (2)$$

where ε_r is the dielectric constant, which has been estimated to 1.22 for phtalocyanines.[45] The estimated $\Delta\phi$ is significantly larger than the experimental value of 0.4 eV, which indicates that the molecules might either be not densely packed and/or few molecules in the second layer might adapt opposite orientation. Nevertheless, we may relate the increase of the work function between 8 and 24 Å to aligned dipole moments pointing toward the surface that originate from molecules of the second layer.

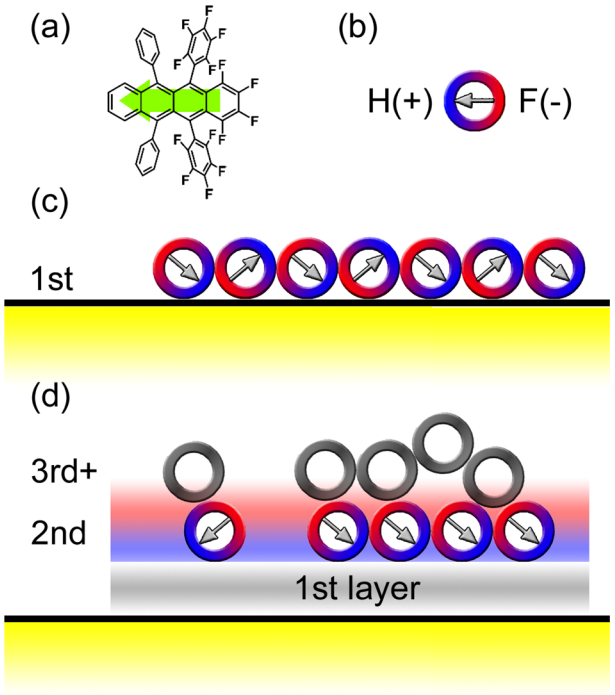

Figure 8. (a) Chemical structure of F_{14}-RUB with a green arrow indicating the direction of the electrostatic dipole moment. (b) Schematic of the polar F_{14}-RUB molecule, the arrow indicates the direction of its static dipole moment, pointing from the fluorinated (−, red) part toward the hydrogenated (+, blue) side. (c) Proposed growth model for F_{14}-RUB on Au(111) and Ag(111). The first layer consists of alternating dipoles, which leads to a canceling out of an overall effective dipole moment perpendicular to the substrate. This is different for the second layer: A majority of the molecular dipole moments is oriented and pointing with the fluorinated part of the molecules away from the substrate. In the third and further layers there is no preferential orientation of the molecules, and the dipole moment from the second layer becomes shielded.

Increasing the film thickness above 24 Å leads to a slight decrease of the work function, which will reach saturation for thick films. This indicates an arrangement of the molecules without preferential orientation, which on one hand does not provide a resulting dipole moment and at the same time slightly screens the dipole moment of the molecules in the second layer.

Our model is corrobated by the progression of the HIB, which is defined by the relative position of the HOMO onset closest to the Fermi level. Below 8 Å only one HOMO peak can be observed for which no clear trend can be identified (cf. Figure 2c and Figure 7a). This corresponds to disordered molecules in the first molecular layer. Between 16 and 20 Å the formerly mentioned second peak appears. This new peak can be assigned to the HOMO of uniformly oriented molecules.[23,28,30] In our interpretation, the reason why we observe this peak only halfway through the formation of the second layer is that the intensity of this peak is too low to be observed below 16 Å. With increasing film thickness the position of the new peak is nearly constant but changes its intensity. Consistent with our model the new HOMO completely disappears for thicker films because the second layer gets more and more covered by higher layers without preferred molecular orientation that attenuate the signal from the new HOMO.

DOI: 10.1021/jp511822g
J. Phys. Chem. C XXXX, XXX, XXX−XXX

CONCLUSION

Concluding, we determined the electronic properties of PF-RUB and F_{14}-RUB thin films deposited on Au(111) and Ag(111). We determined the HIB of PF-RUB and F_{14}-RUB showing the tunability of the HIB of RUB by means of fluorination. The growth mode of the partially fluorinated F_{14}-RUB, which has a large dipole moment along its backbone, turns out to be more complex than for RUB or PF-RUB. We find stronger island growth and, importantly, evidence for a uniform molecular orientation in the second deposited layer for F_{14}-RUB. This leads to an essential modification of the work function and the HOMO level, depending on the film thickness. As a consequence, particularly the partially fluorinated F_{14}-RUB turns out to be a promising candidate for effective tuning of organic interfaces, which is of very high interest for organic optoelectronic devices.

AUTHOR INFORMATION

Corresponding Author

*E-mail: Frank.Schreiber@uni-tuebingen.de.

Notes

The authors declare no competing financial interest.

ACKNOWLEDGMENTS

We acknowledge the financial support of the seventh framework programme (FP7) of the European Union, the Helmholtz Energy Alliance “Hybrid Photovoltaics”, and from the DFG. We thank BESSY II for the technical support at the facility.

REFERENCES

(1) Podzorov, V.; Menard, E.; Borissov, A.; Kiryukhin, V.; Rogers, J. A.; Gershenson, M. E. Intrinsic Charge Transport on the Surface of Organic Semiconductors. *Phys. Rev. Lett.* **2004**, *93*, 086602.

(2) Sundar, V. C.; Zaumseil, J.; Podzorov, V.; Menard, E.; Willett, R. L.; Someya, T.; Gershenson, M. E.; Rogers, J. A. Elastomeric Transistor Stamps: Reversible Probing of Charge Transport in Organic Crystals. *Science* **2004**, *303*, 1644−1646.

(3) Takeya, J.; Yamagishi, M.; Tominari, Y.; Hirahara, R.; Nakazawa, Y.; Nishikawa, T.; Kawase, T.; Shimoda, T.; Ogawa, S. Very High-Mobility Organic Single-Crystal Transistors with in-Crystal Conduction Channels. *Appl. Phys. Lett.* **2007**, *90*, 102120.

(4) Takeya, J.; Kato, J.; Hara, K.; Yamagishi, M.; Hirahara, R.; Yamada, K.; Nakazawa, Y.; Ikehata, S.; Tsukagoshi, K.; Aoyagi, Y.; Takenobu, T.; Iwasa, Y. In-Crystal and Surface Charge Transport of Electric-Field-Induced Carriers in Organic Single-Crystal Semiconductors. *Phys. Rev. Lett.* **2007**, *98*, 196804.

(5) Witte, G.; Wöll, C. Molecular Beam Deposition and Characterization of Thin Organic Films on Metals for Applications in Organic Electronics. *Phys. Status Solidi A* **2008**, *205*, 497−510.

(6) *The Molecule-Metal Interface*; Koch, N., Ueno, N., Wee, A. T. S., Eds.; Wiley VCH-Verlag: Weinheim, Germany, 2013.

(7) Heimel, G.; Duhm, S.; Salzmann, I.; Gerlach, A.; Strozecka, A.; Niederhausen, J.; Bürker, C.; Hosokai, T.; Fernandez-Torrente, I.; Schulze, G.; Winkler, S.; Wilke, A.; Schlesinger, R.; Frisch, J.; Bröker, B.; Vollmer, A.; Detlefs, B.; Pflaum, J.; Kera, S.; Franke, K. J.; Ueno, N.; Pascual, J. I.; Schreiber, F.; Koch, N. Charged and Metallic Molecular Monolayers through Surface-Induced Aromatic Stabilization. *Nat. Chem.* **2013**, *5*, 187−194.

(8) Heimel, G.; Salzmann, I.; Duhm, S.; Koch, N. Design of Organic Semiconductors from Molecular Electrostatics. *Chem. Mater.* **2011**, *23*, 359−377.

(9) Gerlach, A.; Hosokai, T.; Duhm, S.; Kera, S.; Hofmann, O. T.; Zojer, E.; Zegenhagen, J.; Schreiber, F. Orientational Ordering of Nonplanar Phthalocyanines on Cu(111): Strength and Orientation of the Electric Dipole Moment. *Phys. Rev. Lett.* **2011**, *106*, 156102.

(10) Kera, S.; Yabuuchi, Y.; Yamane, H.; Setoyama, H.; Okudaira, K. K.; Kahn, A.; Ueno, N. Impact of an Interface Dipole Layer on Molecular Level Alignment at an Organic−Conductor Interface Studied by Photoemission Spectroscopy. *Phys. Rev. B* **2004**, *70*, 085304.

(11) Fukagawa, H.; Hosoumi, S.; Yamane, H.; Kera, S.; Ueno, N. Dielectric Properties of Polar−Phthalocyanine Monolayer Systems with Repulsive Dipole Interaction. *Phys. Rev. B* **2011**, *83*, 085304.

(12) Delgado, M. C. R.; Pigg, K. R.; da Silva Filho, D. A.; Gruhn, N. E.; Sakamoto, Y.; Suzuki, T.; Osuna, R. M.; Casado, J.; Hernández, V.; Navarrete, J. T. L.; Martinelli, N. G.; Cornil, J.; Sánchez-Carrera, R. S.; Coropceanu, V.; Brédas, J.-L. Impact of Perfluorination on the Charge-Transport Parameters of Oligoacene Crystals. *J. Am. Chem. Soc.* **2009**, *131*, 1502−1512.

(13) de Oteyza, D. G.; Wakayama, Y.; Liu, X.; Yang, W.; Cook, P. L.; Himpsel, F. J.; Ortega, J. E. Effect of Fluorination on the Molecule−Substrate Interactions of Pentacene/Cu(100) Interfaces. *Chem. Phys. Lett.* **2010**, *490*, 54−57.

(14) Uttiya, S.; Raimondo, L.; Campione, M.; Miozzo, L.; Yassar, A.; Moret, M.; Fumagalli, E.; Borghesi, A.; Sassella, A. Stability to Photo-Oxidation of Rubrene and Fluorine-Substituted Rubrene. *Synth. Met.* **2012**, *161*, 2603−2606.

(15) Kera, S.; Hosoumi, S.; Sato, K.; Fukagawa, H.; Nagamatsu, S.-i.; Sakamoto, Y.; Suzuki, T.; Huang, H.; Chen, W.; Wee, A. T. S.; Coropceanu, V.; Ueno, N. Experimental Reorganization Energies of Pentacene and Perfluoropentacene: Effects of Perfluorination. *J. Phys. Chem. C* **2013**, *117*, 22428−22437.

(16) Anger, F.; Scholz, R.; Adamski, E.; Broch, K.; Gerlach, A.; Sakamoto, Y.; Suzuki, T.; Schreiber, F. Optical Properties of Fully and Partially Fluorinated Rubrene in Films and Solution. *Appl. Phys. Lett.* **2013**, *102*, 013308.

(17) Hansson, G.; Flodström, S. Photoemission Study of the Bulk and Surface Electronic Structure of Single Crystals of Gold. *Phys. Rev. B* **1978**, *18*, 1572−1585.

(18) Chelvayohan, M.; Mee, C. H. B. Work Function Measurements on (110), (100), and (111) Surfaces of Silver. *J. Phys. C: Solid State Phys.* **1982**, *15*, 2305−2312.

(19) Duhm, S.; Xin, Q.; Hosoumi, S.; Fukagawa, H.; Sato, K.; Ueno, N.; Kera, S. Charge Reorganization Energy and Small Polaron Binding Energy of Rubrene Thin Films by Ultraviolet Photoelectron Spectroscopy. *Adv. Mater.* **2012**, *24*, 901−905.

(20) Wang, L.; Chen, S.; Liu, L.; Qi, D.; Gao, X.; Wee, A. T. S. Thickness-Dependent Energy Level Alignment of Rubrene Adsorbed on Au(111). *Appl. Phys. Lett.* **2007**, *90*, 132121.

(21) Ding, H.; Gao, Y. Electronic Structure at Rubrene Metal Interfaces. *Appl. Phys. A: Mater. Sci. Process.* **2009**, *95*, 89−94.

(22) Sinha, S.; Mukherjee, M. Thickness Dependent Electronic Structure and Morphology of Rubrene Thin Films on Metal, Semiconductor, and Dielectric Substrates. *J. Appl. Phys.* **2013**, *114*, 083709.

(23) Ding, H.; Reese, C.; Mäkinen, A. J.; Bao, Z.; Gao, Y. Band Structure Measurement of Organic Single Crystal with Angle-Resolved Photoemission. *Appl. Phys. Lett.* **2010**, *96*, 222106.

(24) Ahlrichs, R.; Bär, M.; Häser, M.; Horn, H.; Kölmel, C. Electronic Structure Calculations on Workstation Computers: The Program System Turbomole. *Chem. Phys. Lett.* **1989**, *162*, 165−169.

(25) Scholz, R.; Abbasi, A. Influence of Dispersion Interactions on The Adsorption of PTCDA on Ag(110). *Phys. Status Solidi C* **2010**, *7*, 236−239.

(26) Powell, C. J., Jablonski, A. *NIST Electron Effective-Attenuation-Length Database—Version 1.0*; National Institue of Standards and Technology: Gaithersburg, MD, 2001.

(27) Liu, X.-Q.; Kong, H.-H.; Song, X.; Liu, L.; Wang, L. Ultrathin Monolayer of Rubrene on Au(111) Induced by Charge Transfer. *Surf. Interface Anal.* **2011**, *43*, 1494−1497.

(28) Blüm, M.-C.; Pivetta, M.; Patthey, F.; Schneider, W.-D. Probing and Locally Modifying the Intrinsic Electronic Structure and the

DOI: 10.1021/jp511822g
J. Phys. Chem. C XXXX, XXX, XXX−XXX

Conformation of Supported Nonplanar Molecules. *Phys. Rev. B* **2006**, *73*, 195409.
(29) Lan, M.; Xiong, Z.-H.; Li, G.-Q.; Shao, T.-N.; Xie, J.-L.; Yang, X.-F.; Wang, J.-Z.; Liu, Y. Strain-Driven Formation of Rubrene Crystalline Films on Bi(001). *Phys. Rev. B* **2011**, *83*, 195322.
(30) Glowatzki, H.; Gavrila, G.; Seifert, S.; Johnson, R.; Räder, J.; Müllen, K.; Zahn, D.; Rabe, J.; Koch, N. Hexa-peri-hexabenzocoronene on Ag(111): Monolayer/Multilayer Transition of Molecular Orientation and Electronic Structure. *J. Phys. Chem. C* **2008**, *112*, 1570−1574.
(31) Duhm, S.; Glowatzki, H.; Cimpeanu, V.; Klankermayer, J.; Rabe, J. P.; Johnson, R. L.; Koch, N. Weak Charge Transfer between an Acceptor Molecule and Metal Surfaces Enabling Organic/Metal Energy Level Tuning. *J. Phys. Chem. B* **2006**, *110*, 21069−21072.
(32) Witte, G.; Hänel, K.; Söhnchen, S.; Wöll, C. Growth and Morphology of Thin Films of Aromatic Molecules on Metals: The Case of Perylene. *Appl. Phys. A: Mater. Sci. Process.* **2006**, *82*, 447−455.
(33) Kahn, A.; Koch, N.; Gao, W. Electronic Structure and Electrical Properties of Interfaces between Metals and π-Conjugated Molecular Films. *J. Polym. Sci., Part B: Polym. Phys.* **2003**, *41*, 2529−2548.
(34) Witte, G.; Lukas, S.; Bagus, P. S.; Wöll, C. Vacuum Level Alignment at Organic/Metal Junctions: "Cushion" Effect and the Interface Dipole. *Appl. Phys. Lett.* **2005**, *87*, 263502.
(35) Ito, E.; Oji, H.; Ishii, H.; Oichi, K.; Ouchi, Y.; Seki, K. Interfacial Electronic Structure of Long-Chain Alkane/Metal Systems Studied by UV-Photoelectron and Metastable Atom Electron Spectroscopies. *Chem. Phys. Lett.* **1998**, *287*, 137−142.
(36) Koch, N.; Vollmer, A.; Duhm, S.; Sakamoto, Y.; Suzuki, T. The Effect of Fluorination on Pentacene/Gold Interface Energetics and Charge Reorganization Energy. *Adv. Mater.* **2007**, *19*, 112−116.
(37) Koch, N.; Gerlach, A.; Duhm, S.; Glowatzki, H.; Heimel, G.; Vollmer, A.; Sakamoto, Y.; Suzuki, T.; Zegenhagen, J.; Rabe, J. P.; Schreiber, F. Adsorption Induced Intramolecular Dipole: Correlating Molecular Conformation and Interface Electronic Structure. *J. Am. Chem. Soc.* **2008**, *130*, 7300−7304.
(38) Hill, I. G.; Mäkinen, A. J.; Kafafi, Z. H. Initial Stages of Metal/Organic Semiconductor Interface Formation. *J. Appl. Phys.* **2000**, *88*, 889−895.
(39) Pivetta, M.; Blüm, M.-C.; Patthey, F.; Schneider, W.-D. Coverage-Dependent Self-Assembly of Rubrene Molecules on Noble Metal Surfaces Observed by Scanning Tunneling Microscopy. *Chem. Eur. J. Chem. Phys.* **2010**, *11*, 1558−1569.
(40) Pivetta, M.; Blüm, M.-C.; Patthey, F.; Schneider, W.-D. Three-Dimensional Chirality Transfer in Rubrene Multilayer Islands on Au(111). *J. Phys. Chem. B* **2009**, *113*, 4578−4581.
(41) Miwa, J. A.; Cicoira, F.; Lipton-Duffin, J.; Perepichka, D. F.; Santato, C.; Rosei, F. Self-Assembly of Rubrene on Cu(111). *Nanotechnology* **2008**, *19*, 424021.
(42) Tomba, G.; Stengel, M.; Schneider, W.-D.; Baldereschi, A.; de Vita, A. Supramolecular Self-Assembly Driven by Electrostatic Repulsion: The 1D Aggregation of Rubrene Pentagons on Au(111). *ACS Nano* **2010**, *4*, 7545−7551.
(43) Käfer, D.; Ruppel, L.; Witte, G.; Wöll, C. Role of Molecular Conformations in Rubrene Thin Film Growth. *Phys. Rev. Lett.* **2005**, *95*, 166602.
(44) Wang, L.; Chen, S.; Liu, L.; Qi, D.; Gao, X.; Subbiah, J.; Swaminathan, S.; Wee, A. T. S. Conformational Degree and Molecular Orientation in Rubrene Film by in Situ X-ray Absorption Spectroscopy. *J. Appl. Phys.* **2007**, *102*, 063504.
(45) Fukagawa, H.; Yamane, H.; Kera, S.; Okudaira, K. K.; Ueno, N. Experimental Estimation of the Electric Dipole Moment and Polarizability of Titanyl Phthalocyanine Using Ultraviolet Photoelectron Spectroscopy. *Phys. Rev. B* **2006**, *73*, 041302.

DOI: 10.1021/jp511822g
J. Phys. Chem. C XXXX, XXX, XXX−XXX